



HAL
open science

Characterization of austenitic Stainless steels with regard to environmentally assisted fatigue in simulated light water reactor conditions

Matthias Bruchhausen, Gintautas Dundulis, Alec Mclellan, Sergio Arrieta, Tim Austin, Roman Cicero, Walter John Chitty, Luc Doremus, Miroslava Ernestova, Albertas Grybenas, et al.

► To cite this version:

Matthias Bruchhausen, Gintautas Dundulis, Alec Mclellan, Sergio Arrieta, Tim Austin, et al.. Characterization of austenitic Stainless steels with regard to environmentally assisted fatigue in simulated light water reactor conditions. *Metals*, 2021, 11 (307), pp.20. 10.3390/met11020307. hal-03191106

HAL Id: hal-03191106

<https://hal.science/hal-03191106v1>

Submitted on 6 Apr 2021

HAL is a multi-disciplinary open access archive for the deposit and dissemination of scientific research documents, whether they are published or not. The documents may come from teaching and research institutions in France or abroad, or from public or private research centers.

L'archive ouverte pluridisciplinaire **HAL**, est destinée au dépôt et à la diffusion de documents scientifiques de niveau recherche, publiés ou non, émanant des établissements d'enseignement et de recherche français ou étrangers, des laboratoires publics ou privés.



Distributed under a Creative Commons Attribution 4.0 International License

Article

Characterization of Austenitic Stainless Steels with Regard to Environmentally Assisted Fatigue in Simulated Light Water Reactor Conditions

Matthias Bruchhausen ^{1,*}, Gintautas Dundulis ² , Alec McLennan ³, Sergio Arrieta ^{4,†}, Tim Austin ¹, Román Cicero ⁵, Walter-John Chitty ⁶, Luc Doremus ⁷, Miroslava Ernestova ⁸, Albertas Grybenas ², Caitlin Huotilainen ⁹, Jonathan Mann ¹⁰, Kevin Mottershead ³ , Radek Novotny ¹, Francisco Javier Perosanz ⁴, Norman Platts ³, Jean-Christophe le Roux ¹¹, Philippe Spätig ^{12,13}, Claudia Torre Celeizábal ⁵, Marius Twite ^{10,‡} and Marc Vankeerberghen ¹⁴

- ¹ European Commission, Joint Research Centre, Westerduinweg 3, 1755 LE Petten, The Netherlands; Timothy.AUSTIN@ec.europa.eu (T.A.); radek.novotny@ec.europa.eu (R.N.)
 - ² Lithuanian Energy Institute, Breslaujos 3, LT-44403 Kaunas, Lithuania; gintautas.dundulis@lei.lt (G.D.); albertas.grybenas@lei.lt (A.G.)
 - ³ Jacobs, Faraday Street, Birchwood Park, Warrington WA3 6GA, UK; alec.mclennan@jacobs.com (A.M.); Kevin.Mottershead@jacobs.com (K.M.); norman.platts2@jacobs.com (N.P.)
 - ⁴ Structural Materials Division, Technology Department, Centro de Investigaciones Energéticas, Medioambientales y Tecnológicas (CIEMAT), Avenida Complutense 40, 28040 Madrid, Spain; sergio.arrieta@unican.es (S.A.); franciscojavier.perosanz@ciemat.es (F.J.P.)
 - ⁵ Inesco Ingenieros, CDTUC, Fase B, Av. Los Castros 44, 39005 Santander, Spain; ciceror@inescoingenieros.com (R.C.); claudia.torre@inescoingenieros.com (C.T.C.)
 - ⁶ Institut de Radioprotection et de Sûreté Nucléaire (IRSN), PSN-RES/SEREX/LE2M, CEN de Cadarache, 13115 St. Paul lez Durance, France; walter-john.chitty@irsn.fr
 - ⁷ Framatome, Technical Centre, 30 Bd de l'industrie, 71200 Le Creusot, France; luc.doremus@framatome.com
 - ⁸ UJV REZ, a. s., Hlavni 130, 25068 Husinec, Czech Republic; miroslava.ernestova@ujv.cz
 - ⁹ VTT Technical Research Centre of Finland, Nuclear Reactor Materials, Kivimiehentie 3, 02150 Espoo, Finland; caitlin.huotilainen@vtt.fi
 - ¹⁰ Rolls-Royce, Raynesway P.O. Box 2000, Derby DE21 7XX, UK; jonathan.mann2@rolls-royce.com (J.M.); emmarty@yahoo.com (M.T.)
 - ¹¹ EDF—R&D MMC, Avenue des Renardières—Ecuelles, 77250 Moret-Loing et Orvanne, France; jean-christophe.le-roux@edf.fr
 - ¹² Laboratory for Nuclear Materials, Paul Scherrer Institute, 5232 Villigen-PSI, Switzerland; philippe.spatig@psi.ch
 - ¹³ Laboratory for Reactor Physics and Systems Behaviour, Ecole Polytechnique Fédérale de Lausanne, 1015 Lausanne, Switzerland
 - ¹⁴ SCK CEN, Boeretang 200, 2400 Mol, Belgium; mvankeer@sckcen.be
- * Correspondence: matthias.bruchhausen@ec.europa.eu
† Current address: Laboratory of Materials Science and Engineering (LADICIM), University of Cantabria, E.T.S. de Ingenieros de Caminos, Canales y Puertos, Av. Los Castros 44, Santander, 39005 Cantabria, Spain.
‡ Current address: Emmarty Ltd., Weston-super-Mare BS23 4UL, UK.



Citation: Bruchhausen, M.; Dundulis, G.; McLennan, A.; Arrieta, S.; Austin, T.; Cicero, R.; Chitty, W.-J.; Doremus, L.; Ernestova, M.; Grybenas, A.; et al. Characterization of Austenitic Stainless Steels with Regard to Environmentally Assisted Fatigue in Simulated Light Water Reactor Conditions. *Metals* **2021**, *11*, 307. <https://doi.org/10.3390/met11020307>

Academic Editor: Yun-Jae Kim
Received: 8 December 2020
Accepted: 23 January 2021
Published: 10 February 2021

Publisher's Note: MDPI stays neutral with regard to jurisdictional claims in published maps and institutional affiliations.



Copyright: © 2021 by the authors. Licensee MDPI, Basel, Switzerland. This article is an open access article distributed under the terms and conditions of the Creative Commons Attribution (CC BY) license (<https://creativecommons.org/licenses/by/4.0/>).

Abstract: A substantial amount of research effort has been applied to the field of environmentally assisted fatigue (EAF) due to the requirement to account for the EAF behaviour of metals for existing and new build nuclear power plants. We present the results of the European project INcreasing Safety in NPPs by Covering Gaps in Environmental Fatigue Assessment (INCEFA-PLUS), during which the sensitivities of strain range, environment, surface roughness, mean strain and hold times, as well as their interactions on the fatigue life of austenitic steels has been characterized. The project included a test campaign, during which more than 250 fatigue tests were performed. The tests did not reveal a significant effect of mean strain or hold time on fatigue life. An empirical model describing the fatigue life as a function of strain rate, environment and surface roughness is developed. There is evidence for statistically significant interaction effects between surface roughness and the environment, as well as between surface roughness and strain range. However, their impact on fatigue life is so small that they are not practically relevant and can in most cases be neglected. Reducing the environmental impact on fatigue life by modifying the temperature or strain rate leads to an increase of the fatigue

life in agreement with predictions based on NUREG/CR-6909. A limited sub-programme on the sensitivity of hold times at elevated temperature at zero force conditions and at elevated temperature did not show the beneficial effect on fatigue life found in another study.

Keywords: environmentally assisted fatigue (EAF); austenitic stainless steel; nuclear power plant (NPP); light water reactor (LWR); surface roughness

1. Introduction

According to the most recent report of the Intergovernmental Panel on Climate Change (IPCC), “Nuclear energy is a mature low-GHG [green house gas] emission source of baseload power, but its share of global electricity generation has been declining (since 1993). Nuclear energy could make an increasing contribution to low-carbon energy supply, but a variety of barriers and risks exist” [1]. Hence, long-term operation (LTO) of the current fleet of nuclear power plants (NPPs) can make an important contribution to controlling GHG emissions, especially in the short term. However, this requires proper understanding of the relevant damage mechanisms in NPPs.

Environmentally assisted fatigue (EAF) is one of these damage mechanisms; test programmes in Japan, the U.S. and later in Europe have shown that the water environment in NPPs reduces the fatigue life N_f significantly. Nevertheless, EAF was not explicitly taken into account during the construction of the currently operating fleet of NPPs [2,3]. The most recent guidance for EAF assessment is the U.S. regulation NUREG/CR-6909, Rev. 1 [4], in its final version from May 2018, which is based on an extensive collection mainly of Japanese and U.S. data. In that document, the effect of the environment on N_f is described by an environmental factor F_{en} :

$$F_{en} = \frac{N_{f,air,RT}}{N_{f,LWR}} \quad (1)$$

where $N_{f,air,RT}$ is the fatigue life in air at room temperature and $N_{f,LWR}$ the fatigue life in the environment at operating conditions.

However, the low cycle fatigue lives predicted by CR-6909 do not reflect current pressurized water reactor (PWR) plant experience where no failures attributed to environmental fatigue have been observed so far where the loading conditions were known [2]. Furthermore, studies on laboratory specimens found experimental fatigue lives to be longer than predictions based on CR-6909 [5,6]. This indicates that the guidance provided by CR-6909 includes significant conservatism, which could potentially be reduced without loss of operational plant safety. Accordingly, EAF has received much attention in the last few years [5–15].

Work by Chopra et al. presented a recent review with a focus on ASME Code section III [3] where the F_{en} for austenitic stainless steels is described as:

$$F_{en} = \exp(-T^* \dot{\epsilon}^* O^*) \quad (2)$$

T^* , $\dot{\epsilon}^*$ and O^* are functions of the environmental temperature, the positive strain rate and the dissolved oxygen content. Other parameters like surface finish and complex waveforms are not explicitly taken into account, but taken into account through constant subfactors [4].

However, some authors have observed cases where the combined effect of surface finish and the environment is less damaging than might be expected when considering both effects independently [10,11,16]. These findings suggest there might be interaction effects between the surface finish and the environment.

Similarly, a number of studies investigated the influence of the waveform and especially mean strain [8] and hold time periods on environmental fatigue [6,13]. While mean strain did not have a major effect on fatigue life, it turned out that at least under certain

conditions, introducing hold times at some cycles during the fatigue life can extend the fatigue life of austenitic steels in the PWR environment.

The project INCEFA-PLUS (INcreasing Safety in NPPs by Covering Gaps in Environmental Fatigue Assessment) [17] was started in 2015 under the umbrella of the European Horizon 2020 programme to characterize some of this conservatism. It includes a major test programme with more than 250 (mostly strain controlled) fatigue tests in air and a simulated light water reactor (LWR) environment carried out in 11 European laboratories. While most of the tests were carried out according to a single test matrix that was optimized by the design of experiments method, some specific aspects were addressed in separate sub-programmes.

This work describes the test programme in detail and analyses the data from the main programme in which the effects of five test parameters, as well as their two-factor interactions are considered. The most relevant factors and interactions are identified. Two sub-programmes respectively address hold time effects and conditions under which less environmental impact is expected (i.e., smaller F_{en}).

The implications for actual plant assessment were discussed elsewhere [18]. The analyses presented there were based on an earlier data evaluation similar to the one presented here, but based on a slightly smaller database. The conclusions for fatigue assessment in plants are not affected by the small difference in the underlying database.

2. Materials

The large majority (86%) of the tests were carried out on a single batch (XY182 sheet 23201) of 304L stainless steel produced by Creusot Loire Industries. The remaining tests were carried out on a single batch of 321 (8%) and different batches of 304, 304L and 316L. The chemical composition of the different steels is listed in Table 1. All materials were annealed at temperatures between 1050 °C and 1100 °C. The annealing time was 5 h for the 321 material and between 0.4 and 2 h for the other steels.

Table 1. Chemical composition of the different steels (wt.%). The common material (see column “Comment”) was used in the majority of the tests; the other materials were only used by the indicated organizations.

Material	Al	B	C	Co	Cr	Cu	Fe	Mn	Mo	N
304L			0.029		18.00	0.02	bal.	1.86	0.04	0.056
304L	0.029	0.0005	0.026	0.016	18.626	0.046	bal.	1.558	0.227	0.074
316L	0.022	0.001	0.028	0.007	17.562	0.049	bal.	1.779	2.393	0.062
304			0.035	0.05	18.39	0.17	bal.	1.83	0.2	0.079
321	0.109		0.102		18.08	0.048	bal.	1.446	0.023	
Material	Nb	Ni	P	S	Si	Ta	Ti	V	W	Comment
304L		10.00	0.029	0.004	0.37					Common
304L	0.003	9.737	0.0133	0.0005	0.527	0.01				IRSN
316L	0.002	11.947	0.0121	0.0084	0.642	0.01				IRSN
304		8.07	0.031	0.001	0.32				0.05	Jacobs
321		9.79	0.023		0.52		0.61	0.013		UJV

3. Test Programme

The test programme consisted of a main programme and several sub-programmes dedicated to specific questions arising during the project.

The main programme initially aimed at studying the sensitivities of fatigue life N_f to the parameters strain range ε_r (difference between the maximum and minimum strain during the test), mean strain ε_m (strain level in the middle between the minimum and the maximum strain in a test), hold time t_h (period with constant strain), surface roughness R_t and environment E . These parameters were selected based on the interest of the project partners and the EPRI gap report [2]. The main programme was divided into three consecutive phases (see Section 3.1 for details) to be able to refocus the testing once the first trends became apparent in the data. The data from Phase I did not show any effect of mean strain ([19] and Section 3.1.3), and this was dropped in the later phases. The factor mean strain ε_m was introduced as the easiest means to simulate the constant load applied to NPP

components during steady state operation. However, because of shake down early during the test, the mean strain did not have a significant effect on fatigue life. A sub-programme was started to simulate the constant load via tests with mean stress under strain control. The results of this sub-programme were published separately [20].

It also became apparent that applying hold times during some cycles in this study did not have a major effect on fatigue life. However, significant effects of hold times on fatigue life were reported in a different study [13]. To investigate whether differences in the application of holds led to these differences, a limited sub-programme on hold time tests was started (Section 3.3).

Furthermore, a small test programme with conditions where less environmental effects were expected (i.e., smaller F_{en}) than in the main programme was performed (Section 3.2).

In the absence of a dedicated standard for EAF tests in LWR conditions, the tests were performed as much as possible according to ISO 12106:2017, the standard for strain controlled fatigue testing [21] with additional guidance taken from other relevant standards such as ASTM E606 [22], ISO 11782-1 [23], BS7270:2006 [24] and AFNORA03-403 [25]. To reduce the scatter caused by differences in testing practices between the different laboratories, further guidelines were developed that provide more detailed guidance than is normally included in a testing standard [26]. All test data were uploaded in a dedicated materials database operated by the European Commission (MatDB) and have received digital object identifiers (DOIs) to ensure long-term storage and traceability.

As an additional quality assurance measure, each test was validated by a panel of fatigue experts from within the project and rated with regard to the quality of the test and the completeness of the information in the database. The test quality was determined on the basis of data like the cyclic stress amplitudes and hysteresis curves [26]. Where necessary, this information was complemented by microstructural characterization of the specimens [27]. From the strain controlled tests carried out during the project, ninety-four percent received a quality rating of one or two (out of four) and were accepted without restriction for analysis.

Besides these tests on uni-axial specimens, the project included also a sub-programme on membrane specimens. The results of this sub-programme were published separately [28].

3.1. Main Programme

3.1.1. Test Conditions

The main test programme addressed the influences of the factors strain range ϵ_r , hold time t_h , surface roughness characterized by the total height of the roughness profile R_t , mean strain ϵ_m and environment on the fatigue life of austenitic stainless steels. Preliminary data analyses yielded no indications of significant effects of mean strain and hold times on N_f and were removed during the later phases of the test programme.

Each of the three test phases was optimized by means of the design of experiments (DOE) method [29]. As usual for experimental campaigns for linear models optimized by DOE, all factors were tested on two levels. In the case of continuous factors (like strain range), the minimum and maximum values in the interval of interest were chosen. Using the extreme values maximizes the sensitivity of the test result on the factor settings (because of the higher leverage of the extreme values compared to intermediate values). The only exception from this rule is the surface roughness: While all smooth specimens have a very similar surface roughness, the grinding process used to obtain the rougher surface finishes yielded a roughness distribution rather than a discrete value (Section 3.1.2). For categorical factors like hold time, the two levels were “without holds” and “with holds”.

Table 2 lists the test conditions applied in the main programme. The test conditions were selected to be as plant relevant as possible while keeping test durations realistic (especially for hold times and minimum strain range). The surface roughness is characterized for all specimens by the maximum roughness height R_t and average roughness R_a as specified in ISO 4287:1997 [30]. The smooth surface finishes achieved by polishing

were very reproducible, so not all specimens were measured individually, and generic roughness values were used for most polished specimens. Because of the larger scatter in the surface roughnesses of the rough specimens, R_a and R_t for all ground specimens were measured individually by optical confocal profilometry according to ISO 4288:1997 [31]. In this work, R_t is used rather than R_a because that is the parameter that can be expected to have more impact on crack initiation: a deeper scratch leads to larger stress concentration, which facilitates crack initiation. As both values are strongly correlated (Figure 1), the choice of the surface characteristic is not expected to have a major impact on the analysis.

Table 2. Test conditions in the main programme and the sub-programme on low F_{en} testing.

Parameter	Low Level	Middle Level	High Level	Comment
ε_r (%)	0.6		1.2	
ε_m (%)	0		0.5	only for Phase I
R_t (μm)	0.76	≈ 20	>40	$R_t > 40$ for Phase II only
t_h (h)	0		72	0 or 3 holds of 72 h at mean strain; cycles with holds depend on test conditions
$\dot{\varepsilon}$ (%/s)	0.01		0.1	rising $\dot{\varepsilon}$ in PWR env., falling $\dot{\varepsilon}$ and air tests may vary; $\dot{\varepsilon} = 0.1$ %/s in low F_{en} tests only
T ($^{\circ}\text{C}$)	230		300	$T = 230$ $^{\circ}\text{C}$ in low F_{en} tests only

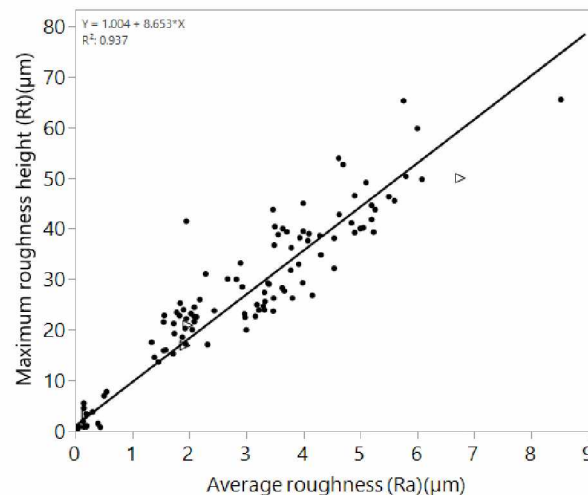


Figure 1. Correlation between R_t and R_a for the specimens in the database (throughout this work, the symbol \triangleright indicates runout specimens). The ratio between R_t and R_a is 8.7.

The PWR and VVER (a Russian PWR design) chemistries are defined in Table 3. In some cases, slightly different water chemistries were used because of different practices in the national power plants. These differences are not expected to have a significant impact on fatigue life, but are recorded in the central database. All tests with the material 321 (and only these) were performed in the VVER environment.

Table 3. Definition of the water chemistry; σ_e is the electric conductivity; DH2 and DO are the dissolved hydrogen and oxygen contents.

Reactor	T $^{\circ}\text{C}$	p MPa	pH @ 300 $^{\circ}\text{C}$	Li ppm	B ppm	K ppm	NH_3 ppm	DH2 cc(STP) H_2/kg	DO ppb	σ_e @ 25 $^{\circ}\text{C}$ $\mu\text{S}/\text{cm}$
PWR	300	15	6.95	2	1000			25	<5	30
VVER	300	12.5	7		1189	16.4	9.7	2	22	80–110

According to CR-6909, the F_{en} for austenitic stainless steels can be formulated as [4]:

$$F_{en} = \exp(-T^* \varepsilon^* O^*) \quad (3)$$

where T^* , $\dot{\epsilon}^*$ and O^* are the parameters derived from temperature, strain rate and dissolved oxygen content. For the conditions used in this work (Tables 2 and 3), these are defined as:

$$T^* = (T - 100)/250 \quad \text{where } T \text{ is in } ^\circ\text{C} \quad (4)$$

$$\dot{\epsilon}^* = \ln(\dot{\epsilon}/7) \quad \text{where } \dot{\epsilon} \text{ is in } \%/s \quad (5)$$

$$O^* = 0.29 \quad (6)$$

For the test conditions in the main programme ($T = 300\text{ }^\circ\text{C}$, $\dot{\epsilon} = 0.01\text{ }1/s$, Tables 2 and 3), Equation (3) yields $F_{en} = 4.57$.

3.1.2. Data Overview

Figure 2 shows the 170 tests that were included in the analysis of the data from the main programme [32]. Four of these tests were runouts, i.e., tests that were stopped for other reasons than specimen failure. These tests are considered as right censored data in the analysis. The mean air curve for austenitic steels from NUREG/CR-6909 [4] and the same curve divided by the F_{en} are plotted for reference.

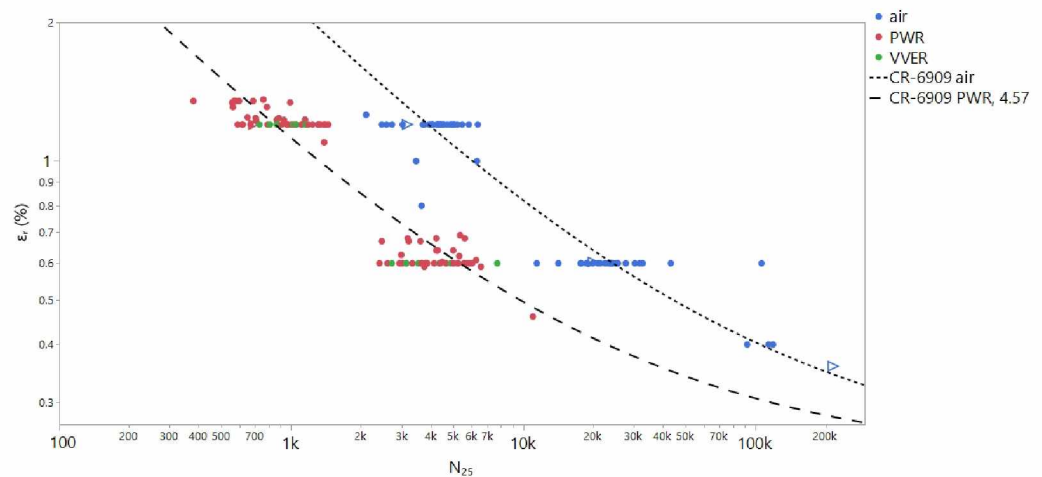


Figure 2. Data from the main programme ($F_{en} = 4.57$). The colours refer to the test environment. The ▷ indicate runouts, i.e., tests that were stopped before specimen failure (e.g., because of a technical problem with the test rig).

The definition of fatigue life N_f used in this study is N_{25} , i.e., the cycle where a reduction of the maximum cyclic stress of 25% compared to the extrapolated stabilized behaviour occurs. In cases where N_X values other than N_{25} are reported, these were converted to N_{25} by means of Equation (18) in NUREG/CR-6909 [4]:

$$N_{25} = \frac{N_X}{0.947 + 0.00212X} \quad (7)$$

While the majority of the tests in the environment were carried out using solid specimens in autoclaves, some data were acquired on hollow specimens where the water flows through the specimen. For hollow specimens, N_f is generally the cycle where leakage occurs. This is considered a rough equivalent to N_{25} [4].

Each organization used their own specimen type and geometry. For the air tests, the specimen diameters varied between 3.6 and 10.0 mm; the solid specimens for the tests in the environment had diameters between 3.6 and 9.0 mm. The hollow specimens had inner diameters between 9 and 12 mm.

Because of the internal pressure in hollow specimens, the stress state in hollow specimens is different from the membrane stress in solid specimens. It is therefore not obvious that the fatigue lives obtained with both types of specimens can be compared

directly [33–35]. A study carried out within INCEFA-PLUS led to the conclusion that no significant effect on the mean values is expected for the data discussed here [36] (this analysis was done on an earlier (smaller) data set, but has been confirmed with the final dataset). Therefore, no further distinction between the two types of specimens is made here. For hollow specimens, the strains are used directly as measured, and no strain correction as suggested in [35] was applied.

The distribution of the independent variables in the main programme is summarized in Figure 3. The relatively low number of tests with a positive mean strain ε_m and a positive hold time t_h reflects the fact that these parameters were dropped in Test Phases II and III, respectively (Table 2).

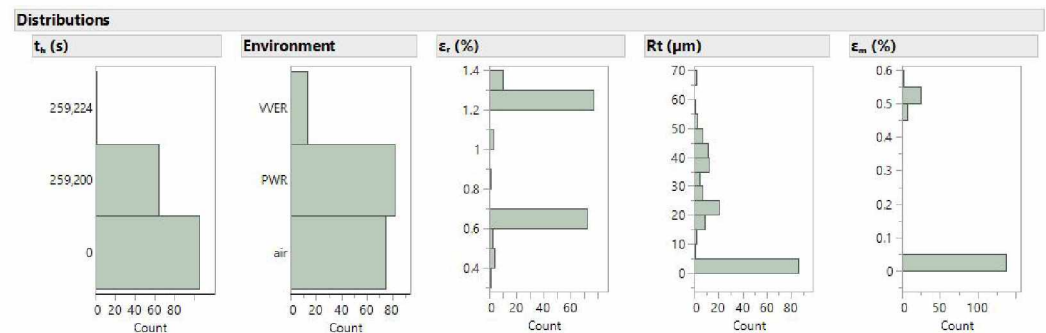


Figure 3. Distribution of the factors in the main programme.

3.1.3. Data Analysis

Before starting the actual data analysis, it is useful to check for possible correlations. The correlation $r_{i,j}$ between the input parameters x_i and x_j is given by:

$$r_{i,j} = \frac{\sum(x_i - \bar{x}_i)(x_j - \bar{x}_j)}{\sqrt{\sum(x_i - \bar{x}_i)^2} \sqrt{\sum(x_j - \bar{x}_j)^2}} \quad (8)$$

where \bar{x} is the mean of x . The correlation $r_{i,j}$ can take values in the interval $[-1;1]$. Values of $|r_{i,j}|$ close to 1 indicate strong (anti-)correlations. If $|r_{i,j}|$ is close to 0, x_i and x_j are not correlated. A strong correlation between x_i and x_j means that tests with high values of x_i also tend to have high values for x_j . Similarly, a strong anticorrelation between x_i and x_j means that high values for x_i are often associated with low values for x_j . Strong (anti-)correlations between the inputs can easily lead to the wrong conclusions during the evaluation because the associated effects cannot be separated.

The three phases of the main test programme were optimized by the design of experiments method [29], which also minimises the correlation between the factors. However, the available collection of tests varied from the planned test matrix, since some tests were invalid or not carried out as specified. Furthermore, additional data were contributed by some project partners, and some test conditions were modified during the project. These circumstances could have introduced correlations between the independent variables.

Table 4 lists the correlations between the factors in the main programme. The largest (anti-)correlations were found between ε_m and R_t and between ε_r and R_t . An anticorrelation between ε_m and R_t was expected since in Phases II and III, no tests with holds were carried out any more, whereas in Phase II, a higher surface roughness R_t was introduced. Therefore, one would expect tests with holds to have on average lower R_t and hence an anticorrelation between R_t and t_h . The correlation between ε_r and R_t , however, is unexpected. Most likely, it is a random effect resulting from the grinding process that was used to produce the rough surface finishes and that yielded a distribution of surface roughnesses rather than specific R_t values (Figure 3). These two largest (anti-)correlations were below 0.15 and should not have a major impact on the evaluation.

Table 4. Correlations between the factors in the main programme

	ε_r	ε_m	R_t	t_h	E
ε_r	1.0000	−0.0183	0.1443	0.0252	0.0492
ε_m	−0.0183	1.0000	−0.1402	−0.0168	−0.0089
R_t	0.1443	−0.1402	1.0000	0.0952	−0.0094
t_h	0.0252	−0.0168	0.0952	1.0000	0.0409
E	0.0492	−0.0089	−0.0094	0.0409	1.0000

The actual data analysis was based on a second degree factorial model, i.e., a model including the main effects and all second order interactions:

$$\ln(N_f) = \sum_i \alpha_i x_i + \sum_{i<j} \alpha_{ij} x_i x_j + I \quad (9)$$

The x_i are the different factors (such as R_t). The parameters α_i and α_{ij} are the model parameters for the main effects and the two factor interactions, and I is the intercept. For every test, an equation like Equation (9) is formulated. The best model is the model for which the parameters α_i , α_{ij} and I best describe the experimental data. A lognormal distribution for N_f is assumed as recommended in ISO 12107 [37]. In a lognormal distribution, the expected (i.e., mean) value \bar{X} of the lognormally distributed variable X is:

$$\bar{X} = \exp\left(\mu + \frac{\sigma^2}{2}\right) \quad (10)$$

μ and σ are the mean and standard variation of the natural logarithm of X .

The model parameters in Equation (9) depend on the scaling of the factors x_i . Normalizing the factors to the range $[-1;1]$ allows comparing the impact of the different main and interaction effects by simply comparing the corresponding α parameters. Table 5 lists the normalization conventions for the factors in the main programme. In this work, the superscript “(n)” indicates normalized factors, e.g., R_t^n is the normalized R_t . For consistency, also the categorical factors like the environment E are labelled similarly (E^n).

Table 5. Normalization of the factors in the main programme.

Factor	Low Value (−1)	High Value (1)	Comment
ε_r (%)	0.6	1.2	min. and max. values according to the test matrix
ε_m (%)	0	0.5	min. and max. values according to the test matrix
R_t (μm)	0.194	65.5	min. and max. values in the dataset
t_h	no hold	incl.holds	categorical variable indicating if the test had holds (Table 2)
E	air	PWR, VVER	categorical variable indicating the environment

The aim of the current study is not only to obtain a numerical model that allows predicting the fatigue life of a specimen under a specific set of test conditions, but especially to determine which of the investigated factors have a significant impact on fatigue life. Therefore, the selected model should not only describe the data, but also include only those variables that have a significant effect on fatigue life. Many algorithms are available for fitting a model to the data. For the present study, we chose the backward elimination [38] method. This algorithm starts with a full model, including all factors and interactions that are being considered (in this case, a second order factorial model, Equation (9)) and evaluates the predictive performance of this model. In the next step, one model parameter (main effect or interaction) is removed, and the performance of the reduced model is evaluated. This procedure is repeated iteratively until only the intercept is left. This approach allows more easily comparing models with different numbers of factors than is the case for other algorithms that do not eliminate factors at all or where the number of factors is not changed in every step.

The model that best fits the data is not necessarily the most useful model since models with more parameters can easily overfit the data (i.e., fit the noise). Two approaches were used here for model selection. In the first approach, the data set is divided into a training set and a validation set. The data in the training set are used to determine the model parameters α_i . The data in the validation set are then used to evaluate the predictive performance of the model. Since the data in the validation set were not used to determine the model parameters, the predictive performance of the model on the validation set is a good measure for the model performance under new conditions within the parameter range in which the model was optimized.

From Figure 2, it is clear that the data sets can be roughly separated into four distinct groups by the two levels of ε_r and E . The training and validation sets are selected in such a way that 75% of the data in each of the four groups are in the training set and 25% in the validation set. This approach is shown in Figure 4a, where the $-\text{LogLikelihood}$ for the training and the validation sets is plotted over the iteration steps of the algorithm. The $-\text{LogLikelihood}$, the negative natural logarithm of the likelihood function, is a measure for the goodness of fit, whereby smaller numbers indicate a better fit. The iteration steps of the algorithm start with Step Number 0, i.e., the full model including all main effects and all two parameter interactions. Moving on the abscissa left allows following the progression of the algorithm until at the leftmost step (here, Step 15), only the intercept remains.

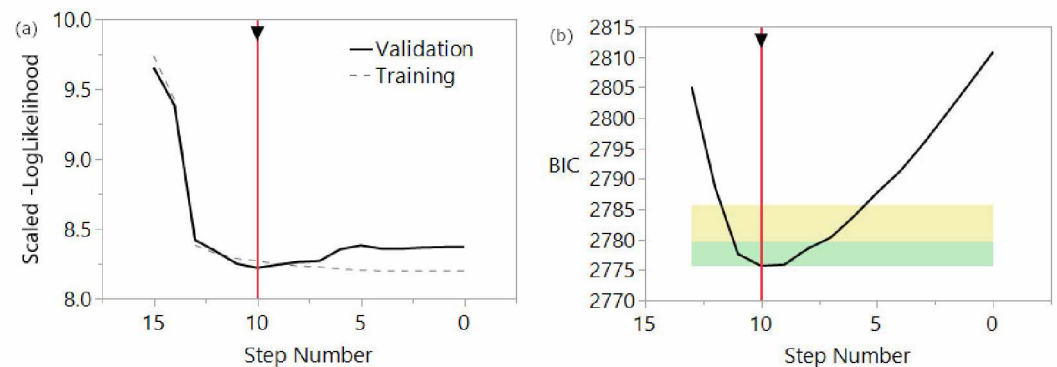


Figure 4. Comparison of the model performances as a function of the step in the algorithm, i.e., the number of factors that were removed from the model. Note that progression on the abscissa is from right to left. The vertical red line indicates the optimal model according to the algorithm. (a) $-\text{LogLikelihood}$ for the training and validation sets. (b) BIC for the full data set; the green area indicates “very good” model performance (strong evidence that a model is comparable to the best model); the yellow area indicates “good” model performance (weak evidence that a model is comparable to the best model) [39].

The dashed line refers to the training set. The $-\text{LogLikelihood}$ for the training set rises continuously with the progression of the algorithm (from right to left). This is expected since reducing the number of terms in the model will necessarily lead to worse fits. The behaviour of the solid curve for the validation set is different: initially, the $-\text{LogLikelihood}$ drops until it reaches a minimum in Step 10 (indicated by the vertical red line) and continuously rises from there. This means that the model that best describes the validation set is reached in Step 10 of the algorithm. The corresponding model coefficients are listed in Table 6 Model (a) (Appendix A).

An alternative approach for selecting a model and to avoid overfitting is using a measure for the quality of the fit that penalises models with a larger number of parameters. The Bayesian information criterion (BIC) is such a measure. It is defined as:

$$\text{BIC} = -2\text{LogLikelihood} + k \ln(n) \quad (11)$$

where k is the number of parameters in the model and n the number of data points. As for the $-\text{LogLikelihood}$ discussed above, lower values of BIC indicate a better fit. The second

term of the sum in Equation (11) penalizes models with more parameters. Figure 4b shows the BIC for the different steps in the backward elimination algorithm for the full data set. The best model is again reached in Step 10; the corresponding model coefficients are listed in Table 6 Model (b).

Table 6. Coefficients for the best models in Figure 4. Note that the normalized versions of the factors need to be used (Table 5); in the case of the categorical variable E^n the coefficient is zero for $E^n = -1$ and the value in the table for $E^n = +1$. The p -value in the last column is an indication of the statistical significance of an effect; a threshold of 0.05 is often used as criterion for statistical significance with lower values indicating higher significance. σ is a parameter in the lognormal distribution (Equation (10)).

Model	Factor	Estimate	Std Error	p -Value
Model (a)	I	9.170	0.04524	<0.0001
	ε_r^n	−0.9011	0.04644	<0.0001
	$E^n [+1]$	−1.637	0.05123	<0.0001
	R_t^n	−0.1995	0.04137	<0.0001
	$(\varepsilon_r^n - 0.06958) * E^n [+1]$	0.1444	0.05558	0.0094
	$(\varepsilon_r^n - 0.06958) * (R_t^n + 0.51401)$	0.09537	0.04329	0.0276
	σ	0.2850	0.02844	<0.0001
Model (b)	I	9.157	0.04059	<0.0001
	ε_r^n	−0.9355	0.04578	<0.0001
	$E^n [+1]$	−1.637	0.04594	<0.0001
	R_t^n	−0.2169	0.03702	<0.0001
	$(\varepsilon_r^n - 0.06958) * E^n [+1]$	0.1766	0.05218	0.0007
	$(\varepsilon_r^n - 0.06958) * (R_t^n + 0.51401)$	0.1097	0.04005	0.0062
	σ	0.2913	0.02543	<0.0001

3.1.4. Discussion

Comparing the model coefficients listed in Table 6 Models (a) and (b) shows that both models include the same terms, namely the main effects ε_r^n , E^n and R_t^n , as well as the two interactions $\varepsilon_r^n * E^n$ and $\varepsilon_r^n * R_t^n$. The estimates for the coefficients of all three main effects are negative, indicating their detrimental effect on fatigue life.

The estimated factor for the interaction $\varepsilon_r^n * E^n$ is positive; large values for either ε_r^n or E^n , i.e., large strain ranges or testing in the LWR environment therefore partly compensate the negative effects of ε_r^n and E^n ; at high strain ranges, there is less environmental effect. This is consistent with the observation reported in [3].

Similarly, the positive coefficient related to the interaction term $\varepsilon_r^n * R_t^n$ reduces the negative impact of a high surface roughness at high strain ranges. This is understandable: R_t affects crack initiation rather than crack growth, so one would expect R_t to have a more deleterious impact in situations where fatigue life is dominated by crack initiation, i.e., at low strain ranges, which is what the models predict.

Models (a) and (b) were determined using the same algorithm (backward elimination), but with different validation methods. Published and project internal analyses with different algorithms and slightly different data sets consistently showed the main effects ε_r , E and R_t to have the largest impact [40]. In most cases, one or two two-factor interactions were found to be statistically significant, but not practically relevant, i.e., they did not have a major impact on the predicted fatigue life. The interactions that were found to be statistically significant varied in evaluations with increasing size of the data set and depending on the algorithm used for the model optimization. This may indicate that the size of these effects is at the limit of what is detectable with the number of tests available in this work.

This is confirmed by the optimization curves (the solid black lines) for both models in Figure 4. In both cases, the best model is found in Step 10, but the performance of the models in Step 9 or 11 is very comparable. A further reduced model, including only the

main effects, was therefore calculated (using the BIC validation); the model parameters are listed in Table 7.

Table 7. Coefficients for a reduced model including only the main effects. Note that the normalized versions of the factors need to be used (Table 5); in the case of the categorical variable E^n the coefficient is 0 for $E^n = -1$, and the value in the table for $E^n = +1$.

Model	Factor	Estimate	Std Error	p-Value
Model (c)	I	9.173	0.04283	<0.0001
	ϵ_T^n	-0.8354	0.02690	<0.0001
	$E^n [+1]$	-1.650	0.05097	<0.0001
	R_t^n	-0.2160	0.03696	<0.0001
	σ	0.3124	0.03103	<0.0001

Figure 5a compares the N_{25} predicted by the three models to the experimentally observed values. As could be expected from Table 6, Models (a) and (b) are hardly distinguishable. Only at very high N_{25} do differences become apparent. Model (c), which only includes the main effects, differs visibly from the other two models. For high fatigue lives, Model (c) systematically predicts lower N_{25} , whereas the contrary can be observed in the medium N_{25} range around 4000 cycles. In the region where N_{25} is around 1000 cycles, all three models match well in general, with Model (c) deviating from the others in some cases. These differences result from omitting the interaction effects. However, the differences between the reduced model (c) and the optimal models (a) and (b) is small compared to the scatter observed experimentally. Therefore, Model (c) seems to be good enough to make realistic predictions.

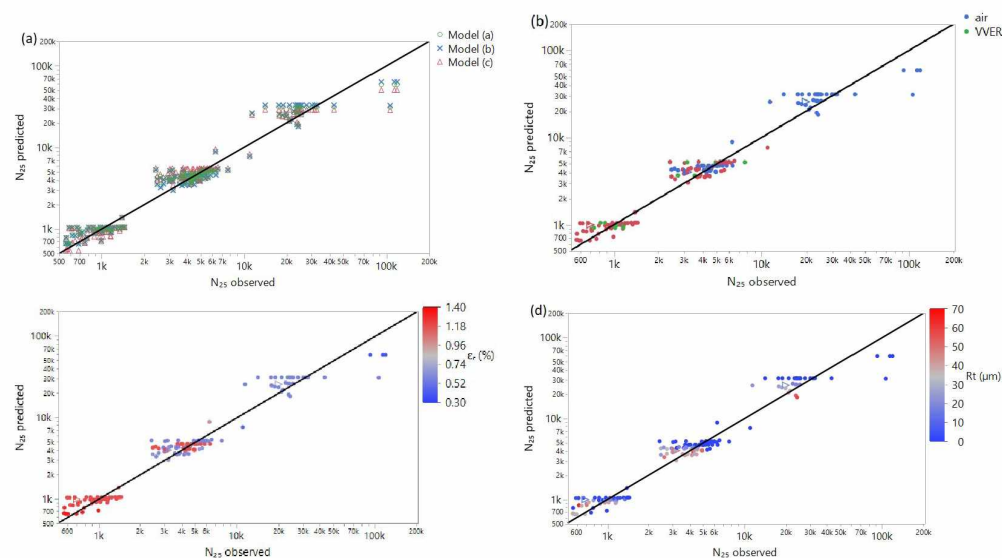


Figure 5. Model predictions for N_{25} vs. experimental values: (a) comparison between the models (a–c). For the predictions with Model (a), colour coding highlights the different environments (b), strain ranges (c) and the surface roughnesses (d).

During the analysis, all tests were considered to be either carried out in air or in the LWR environment, where the LWR environment included simulated PWR, as well as simulated VVER conditions, and no distinction was made between the latter two. Furthermore, all tests in the VVER environment (and only these) were performed on a 321 steel. The question is if considering the PWR and VVER tests was a sensible approach. Figure 5b–d compares the predicted N_{25} from Model (a) to the experimentally observed values, whereby the colour coding indicates the different environments, strain ranges and surface roughnesses.

The VVER data in Figure 5b are distributed around the black reference line and do not show any particularities. Hence, based on the data available here, the model describes the VVER data just as well as the PWR data. Similarly, the model predictions work equally well for different strain ranges ε_r (c) and surface roughnesses R_t (d). The effect of R_t on the predicted fatigue life is visible by the separation of the blue points with very low and the grey/red points with higher R_t values. The gap between these two groups is higher for larger fatigue lives, showing the interaction between R_t and ε_r .

3.2. Sub-Programme on Low F_{en} Conditions

3.2.1. Test Conditions

In this sub-programme, a limited number of tests were carried out at conditions with a lower F_{en} than in the main programme. From Equation (3), it follows that without changing the water chemistry (i.e., the DO content), the approaches that allow reducing F_{en} are reducing the temperature T and increasing the (positive) strain rate $\dot{\varepsilon}$. The maximum strain rate that could be achieved in all autoclaves in the project was an increase by a factor 10 compared to the main programme, i.e., $\dot{\varepsilon} = 0.1\%/s$. This leads to a $F_{en} = 2.68$; the same F_{en} is obtained by reducing T to $230\text{ }^\circ\text{C}$ (Table 2).

3.2.2. Data Overview

Only a limited number of tests was available for the test programme at reduced F_{en} . Here, only tests with a strain range $\varepsilon_r = 0.6\%$ in the LWR environment are considered. Forty-nine tests were available for the analysis [41], of which 15 were at the lower F_{en} , with eight tests at reduced temperature T and seven tests at increased positive strain rate $\dot{\varepsilon}$. Data from the main programme at the positive strain rate $0.01\%/s$ were used as reference data. Some of these tests were carried out with mean strain or hold times. However, since the analysis of the data in the main programme did not reveal any mean strain or hold time effects, these parameters are not considered in context with the low F_{en} data. The fatigue lives of the tests used in the low F_{en} analysis are plotted in Figure 6 and the distributions of the most relevant test parameters in Figure 7.

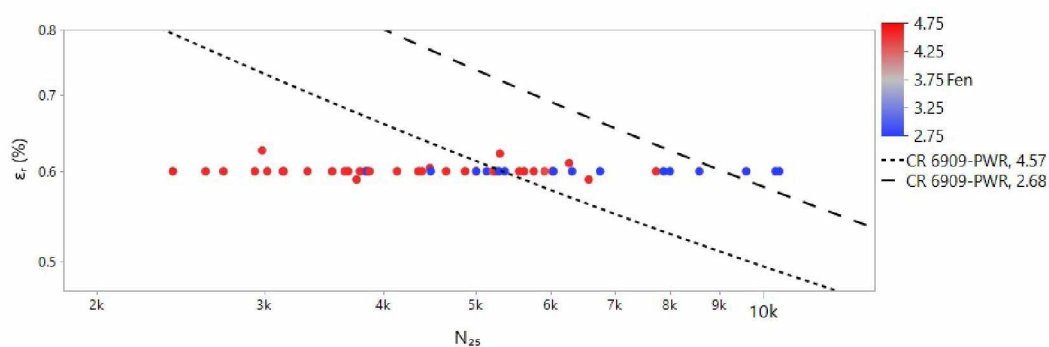


Figure 6. Data in the low F_{en} programme; the reference curves are calculated from the NUREG/CR-6909 mean air curve and the two F_{en} values considered here.

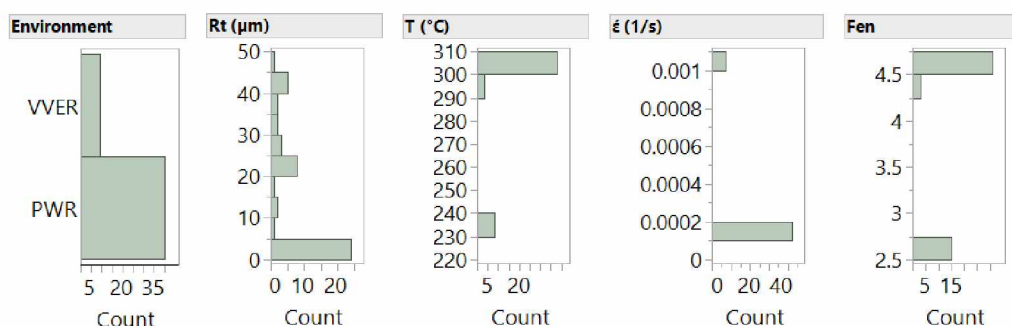


Figure 7. Distribution of the factors in the low F_{en} programme.

3.2.3. Data Analysis

Because of the limited number of tests available for this sub-programme, no tests with reduced temperature T and increased strain rate $\dot{\epsilon}$ were carried out. This gap in the test matrix is reflected in the correlation between T and $\dot{\epsilon}$ in the correlation matrix (Table 8). It should also be noted that the small number of tests led to a reduced spectrum of R_t in the low F_{en} data. For both groups of low F_{en} data (with reduced T and with increased $\dot{\epsilon}$), the maximum R_t is around $30 \mu\text{m}$, whereas for the group at higher F_{en} , it is almost $50 \mu\text{m}$.

Table 8. Correlations between the factors in the low F_{en} programme

	R_t	$\dot{\epsilon}$	T
R_t	1.0000	−0.0589	0.0823
$\dot{\epsilon}$	−0.0589	1.0000	0.1846
T	0.0823	0.1846	1.0000

Table 9 shows the normalization definitions for the factors in the low F_{en} programme. Notice that the spectrum of R_t values is smaller than in the main programme, which leads to a slightly different normalization.

Table 9. Normalization of the factors T and $\dot{\epsilon}$ for the tests at reduced F_{en} .

Factor	Low Value (−1)	High Value (1)	Comment
T ($^{\circ}\text{C}$)	230	302.3	min. and max. values in the dataset
$\dot{\epsilon}$ (1/s)	0.01	0.1	min. and max. values according to test matrix
R_t (μm)	0.335	49.75	min. and max. values in the dataset

The small number of tests available in the two low F_{en} groups makes it impractical to divide the data into a training and a validation set. Therefore, only the BIC method described in Section 3.1.3 is used for the analysis of the low F_{en} data. As before, the optimal model is determined by means of the backward elimination algorithm. The initial model includes all three main effects R_t^n , $\dot{\epsilon}^n$ and T^n , as well as the two-factor interactions $R_t^n * \dot{\epsilon}^n$ and $R_t^n * T^n$. Since no data with high $\dot{\epsilon}$ and low T are available, no information about a possible interaction between these two parameters is present in the data.

The plot with the different steps of the backward elimination algorithm is shown in Figure 8; the parameter estimates for the optimal model, which includes only the main effects, are listed in Table 10.

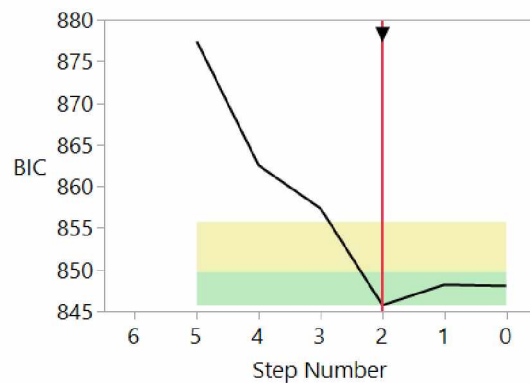


Figure 8. Variation of BIC during the iteration steps of the backward elimination algorithm for the low F_{en} model.

Table 10. Coefficients of the optimal model for the low F_{en} data. Note that the normalized versions of the factors need to be used (Table 9).

Factor	Estimate	Std Error	<i>p</i> -Value
I	8.643	0.05659	<0.0001
R_t^n	−0.2879	0.05369	<0.0001
$\dot{\epsilon}^n$	0.2048	0.05023	<0.0001
T^n	−0.2091	0.03572	<0.0001
σ	0.2303	0.02785	<0.0001

3.2.4. Discussion

As would be expected, higher $\dot{\epsilon}$, as well as lower R_t and T increased the fatigue life. From the coefficients in Table 10, it is clear that increasing $\dot{\epsilon}$ from 0.0001/s to 0.001/s and reducing T from 300 °C to 230 °C had the same beneficial effect on fatigue life. In the range of parameters studied here, the effect of R_t was ca. 40% stronger than that of the other two parameters.

In Table 11, the fatigue lives for polished specimens ($R_t^n = -1$) are calculated for different settings of T^n and $\dot{\epsilon}^n$. The first row corresponds to the conditions in the high F_{en} programme. In the second and third row, the fatigue lives for the two means of reducing the F_{en} are calculated. As expected, reducing T^n and increasing $\dot{\epsilon}^n$ yield virtually the same predicted N_{25} . The ratio between the predicted N_{25} values at low and high F_{en} conditions is 1.5. This is reasonably close to the ratio of the high and low F_{en} values (1.7).

Table 11. Fatigue lives calculated with the model in Table 10.

R_t^n	$\dot{\epsilon}^n$	T^n	N_{25}
−1	−1	1	5131
−1	−1	−1	7794
−1	1	1	7728

Other algorithms led to models that also included the statistically significant interactions $R_t^n * \dot{\epsilon}^n$ and $R_t^n * T^n$. In these models, the coefficient for $R_t^n * \dot{\epsilon}^n$ was negative, and the coefficient for $R_t^n * T^n$ was positive. That would mean that in the parameter range studied here, the fatigue life of polished specimens would be more sensitive to the variations of positive strain rate and temperature than the fatigue life of specimens with a ground surface finish. However, the error bars of the more complex models overlap with the error bars of the simpler model in Table 10 so that from an application point of view, there is no practical difference between the models, and the simpler one can be used.

3.3. Sub-Programme on Hold Times

A series of tests that included hold times was performed in Phases I and II of the INCEFA-PLUS test programme (Section 3.1). The tests on hold time effects in Phases I and II were carried out in strain-control at the strain ranges 0.6% and 1.2% (Table 2). The hold periods were introduced at the position in the cycles where the mean strain (0% or 0.5%) was reached with a positive strain rate. Holds of 72 h were introduced in three cycles per tests; the cycles with holds depended on the test conditions. For tests in air, holds were added at 6000 cycle intervals starting from the 6000th cycle for strain range 0.3% and 1000 cycle intervals starting from the 1000th cycle for 0.6%. Preliminary analysis including Phase II tests ([40,42], confirmed in Section 3.1.3) suggested that there was no observable effect of hold times for the tested conditions, although beneficial effects of hold time on fatigue life have been reported by the AdFaM (Advanced Fatigue Methodologies) project [13].

Therefore, hold times were removed from Phase III testing, and in parallel, a sub-programme on hold time effects was initiated where the test conditions were more closely aligned to those used in the AdFaM study [13].

3.3.1. Data from Hold Time Testing

According to [13], hold time effects were most prominent at low strain amplitude and with holds at zero stress at elevated temperature. To increase the chances of observing a hold time effect, the strain range in the sub-programme on hold time effects therefore was reduced to 0.4%. Furthermore, holds were performed under zero load rather than in strain control (in some cases, at non-zero mean strain) as in the main program. The holds consisted of three 72 h holds at 350 °C at 10,000 cycle intervals starting from the 10,000th cycle. The temperature during hold times was increased from 300 °C to 350 °C. Cycling was carried out at room temperature or at 300 °C. All tests were performed in air on the common batch XY182 of 304L [43].

Figure 9 shows the evolution of the maximum stress per cycle during the test.

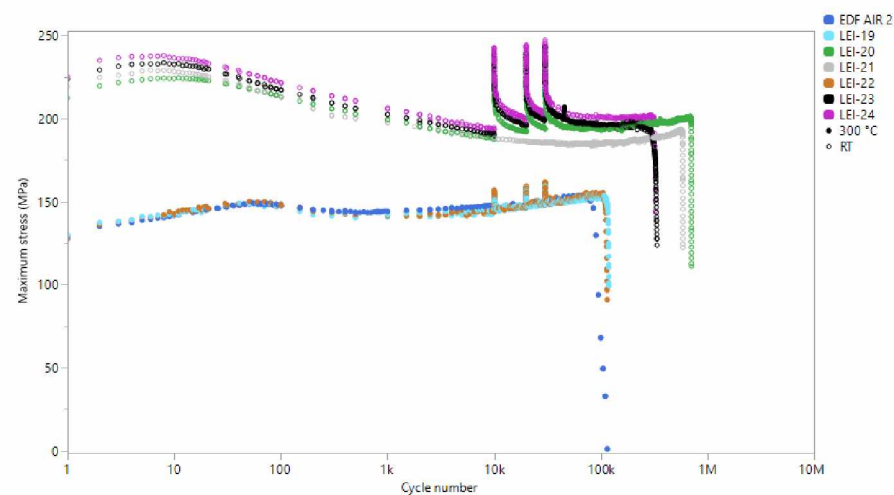


Figure 9. Maximum stress as a function of cycle; all tests were carried out at a strain range of 0.4%. The tests “EDF AIR 2” and “LEI-21” are the only tests that did not have holds.

Three of the seven tests (specimens “EDF AIR 2”, “LEI-19” and “LEI-22”) were carried out at 300 °C, whereas the other four were performed at room temperature. The tests with the specimens “EDF AIR 2” and “LEI-21” were the only ones without holds.

3.3.2. Discussion of Hold Time Data

The reducing effect of the increased temperature on the stress level and fatigue life is obvious from Figure 9. The hardening effect of the hold periods is visible from the

peaks in the maximum stress at 10,000, 20,000 and 30,000 cycles. The curves for the tests at 300 °C showed a primary hardening followed by softening and secondary hardening before failure occurred around Cycle 100000. The maximum cyclic stresses of the three tests evolved in very similar manner—especially given that they were tested in two different laboratories (LEI and EDF). The hold times led to hardening, but there was no long lasting effect in either stress level or fatigue life.

The situation for the tests at room temperature was different: until the first hold at Cycle 10000, the stress curves evolved in parallel even if there were some differences in absolute stress values. The first hold (at 350 °C at zero stress) then hardened the material, similar to what was observed for the tests cycled at 300 °C. However, the stress increase was much higher and decayed more slowly when cycling restarted. Furthermore, for the remainder of the tests, the three tests with holds reached higher stress levels compared to the reference test (“LEI-21”) than they had before the holds. The second and third hold times seemed to have less effect. The increased stress, however, did not seem to have an impact on fatigue life. In particular, no extension of fatigue life as reported in [13] was evident (two of the three tests with holds were actually shorter than the reference test without holds). The reason for that discrepancy with the AdFaM results remains unclear; it might be that the number of hold periods played a role. In the tests reported in [13], hold periods were applied throughout the test, so depending on the conditions, there were many more than just three hold periods in a test.

4. Conclusions

A major test programme on strain controlled fatigue in air and LWR conditions was carried out. The main programme with $F_{en} = 4.57$ investigated the effects of strain range, mean strain, hold time, surface roughness and environment on the fatigue life of austenitic steels. The test matrix was optimized by the design of experiments methodology. A linear model taking into account possible interactions was determined. No influences of hold time and mean strain were identified. The test data could be described by a model including only the main factors strain rate, environment and surface roughness. The interaction effects of strain range with the environment, as well as surface roughness were found to be statistically significant, but of limited practical relevance.

In a sub-programme at a lower $F_{en} = 2.68$, the influences of temperature, positive strain rate, as well as surface roughness were studied. Because of the limited number of tests, not all possible interactions could be addressed. No firm evidence for an interaction of surface roughness with either temperature or strain rate was detected. In the parameter range investigated, the effect of surface roughness was slightly larger than the effects of temperature and strain rate. As predicted by NUREG CR-6909, the reduction of the temperature from 300 °C to 230 °C in the LWR environment was found to have the same effect on fatigue life compared to $F_{en} = 4.57$ as the increase of the positive strain rate from 0.0001/s to 0.001/s.

Finally, a limited number of tests in air with holds at elevated temperature under no stress conditions did not find evidence for beneficial effects of hold times on fatigue life like those found in another study. The reason might be the difference in the number of hold time periods.

Author Contributions: Conceptualization: M.B. methodology: M.B. validation: A.M. formal analysis: M.B., J.M. and A.M. investigation: S.A., R.C., W.-J.C., L.D., G.D., M.E., A.G., C.H., A.M., R.N., F.J.P., N.P., J.-C.I.R., P.S. and M.V. data curation: T.A., M.B., R.C., L.D., C.H., A.M., N.P., J.-C.I.R., P.S., C.T.C., M.T. and M.V. writing—original draft preparation: M.B. and G.D. writing—review and editing: W.-J.C., M.V., A.M., K.M., C.H., G.D. and P.S. project administration: K.M., M.B., R.C., C.H., J.-C.I.R. and M.V. funding acquisition: K.M. and R.C. All authors read and agreed to the published version of the manuscript.

Funding: This project received funding from the Euratom Research and Training Programme 2014-2018 under Grant Agreement No. 662320.

Institutional Review Board Statement: Not applicable.

Informed Consent Statement: Not applicable.

Data Availability Statement: Requests to access the data presented in this study can be submitted to the data owner(s). The data are stored in a database and traceable through DOIs [32,41,43] but are not publicly available due to the data policy of the project.

Conflicts of Interest: The authors declare no conflict of interest. The funders had no role in the design of the study; in the collection, analyses, or interpretation of data; in the writing of the manuscript; nor in the decision to publish the results.

Abbreviations

The following abbreviations and symbols are used in this manuscript:

AdFaM	Advanced Fatigue Methodologies (name of a project)
DOE	design of experiments
EAF	environmentally assisted fatigue
LTO	long-term operation
NPP	nuclear power plant
PWR	pressurized water reactor
VVER	voda-vodyanoi energetichesky reaktor (Russian: pressurized water reactor)
α_i	model parameter
BIC	Bayesian information criterion
DH2	dissolved hydrogen content
DO	dissolved oxygen content
E	categorical variable for environment; either “air” or “LWR”
E^n	normalized categorical variable for environment; either “−1” or “+1”
ε_r	strain range: difference between the maximum and minimum strain during a test
ε_r^n	normalized strain range
$\dot{\varepsilon}$	strain rate
$\dot{\varepsilon}^n$	normalized strain rate
$\dot{\varepsilon}^*$	strain rate parameter defined in CR-6909 [4]
ε_m	mean strain: strain level in the middle between the maximum and minimum strain in a strain controlled test
ε_m^n	normalized mean strain
F_{en}	environmental factor
I	intercept in model
LogLikelihood	natural log of the likelihood function
N_{25}	fatigue life, 25% force drop compared to stabilized linear behaviour
N_f	fatigue life
$N_{f,air,RT}$	fatigue life in air at room temperature
$N_{f,LWR}$	fatigue life in LWR environment
N_X	fatigue life, X% force drop
O^*	dissolved oxygen parameter defined in CR-6909 [4]
$r_{i,j}$	correlation between two variables x_i and x_j
R_a	average surface roughness as defined in ISO 4287 [30]
R_t	maximum roughness height as defined in ISO 4287 [30]
R_t^n	normalized surface roughness R_t
σ_e	electric conductivity
t_h	categorical variable for hold time
t_h^n	normalized hold time
T	temperature
T^n	normalized temperature
T^*	temperature parameter defined in CR-6909 [4]

Appendix A

Algorithms A1 Matlab Function for Model (a)

```
function N25 = model_a(epsn,Rtn,En)
% MODEL_A
% This function calculates the fatigue life according to the model (a) in Table 6
% The entries are the normalized values of strain range, surface
% roughness and environment as in Table 5.

% The coefficients according to Table 6 (a)
% main effects and sigma
I = 9.1695785;
epsn_coeff = -0.90106;
switch En
    case -1
        En_coeff = 0;
    case 1
        En_coeff = -1.637142;
end
Rtn_coeff = -0.199527;
sigma = 0.2849506;

% coefficients and offsets for the interaction terms
% interaction between epsn and En
switch En
    case -1
        epsn_x_En_coeff = 0;
    case 1
        epsn_x_En_coeff = 0.144387;
end
epsn_offset1 = -0.06958;
% interaction between epsn and Rtn
epsn_x_Rtn_coeff = 0.0953654;
epsn_offset2 = -0.06958;
Rtn_offset = 0.51401;

N25 = exp(I + epsn_coeff*epsn + En_coeff*En + Rtn_coeff*Rtn + ...
    epsn_x_En_coeff*(epsn + epsn_offset1)*En + ...
    epsn_x_Rtn_coeff*(epsn + epsn_offset2)*(Rtn + Rtn_offset) + ...
    sigma^2/2);
end
```

References

1. IPCC. Summary for Policymakers. In *Climate Change 2014: Mitigation of Climate Change. Contribution of Working Group III to the Fifth Assessment Report of the Intergovernmental Panel on Climate Change*; Edenhofer, O., Pichs-Madruga, R., Sokona, Y., Farahani, E., Kadner, S., Seyboth, K., Adler, A., Baum, I., Brunner, S., Eickemeier, P., et al., Eds.; Cambridge University Press: Cambridge, UK; New York, NY, USA, 2014.
2. Tice, D.; McLennan, A.; Gill, P. *Environmentally Assisted Fatigue (EAF) Knowledge Gap Analysis: Update and Revision of the EAF Knowledge Gaps*; Technical Report 3002013214; Electric Power Research Institute: Palo Alto, CA, USA, 2018.
3. Chopra, O.K.; Stevens, G.L.; Tregoning, R.; Rao, A.S. Effect of Light Water Reactor Water Environments on the Fatigue Life of Reactor Materials. *J. Press. Vessel. Technol.* **2017**, *139*, 060801. [[CrossRef](#)]
4. Chopra, O.; Stevens, G. *Effect of LWR Coolant Environments on the Fatigue Life of Reactor Materials*; Technical Report NUREG/CR-6909; Rev. 1, U.S. NRC: Rockville, MD, USA, 2018.
5. Seppänen, T.; Alhainen, J.; Arilahti, E.; Solin, J. Low Cycle Fatigue (EAF) of AISI 304L and 347 in PWR Water. In Proceedings of the ASME Pressure Vessels and Piping Conference, Prague, Czech, 15–20 July 2018; PVP2018-84197; Volume 1A.
6. Herbst, M.; Roth, A.; Rudolph, J. Study on Hold-Time Effects in Environmental Fatigue Lifetime of Low-Alloy Steel and Austenitic Stainless Steel in Air and Under Simulated PWR Primary Water Conditions. In Proceedings of the 18th International Conference on Environmental Degradation of Materials in Nuclear Power Systems—Water Reactors, Marriott, Portland, 13–17 August 2017; Jackson, J.H., Paraventi, D., Wright, M., Eds.; Springer International Publishing: Cham, Switzerland, 2019; pp. 987–1006.

7. Métais, T.; Morley, A.; de Baglion, L.; Tice, D.; Stevens, G.; Cuvilliez, S. Explicit Quantification of the Interaction between PWR Environment and Component Surface Finish in Environmental Fatigue Evaluation Methods for Austenitic Stainless Steels. In Proceedings of the ASME Pressure Vessels and Piping Conference, Prague, Czech, 15–20 July 2018; PVP2018-84240; Volume 1A.
8. Kamaya, M. Influence of Mean Strain on Fatigue Life of Stainless Steel in PWR Water Environment. In Proceedings of the ASME Pressure Vessels and Piping Conference, Prague, Czech, 15–20 July 2018; PVP2018-84461; Volume 1A-2018.
9. Tsutsumi, K.; Huin, N.; Couvant, T.; Henaff, G.; Mendez, J.; Chollet, D. Fatigue Life of the Strain Hardened Austenitic Stainless Steel in Simulated PWR Primary Water. In Proceedings of the ASME 2012 Pressure Vessels and Piping Conference, Toronto, ON, Canada, 15–19 July 2012; Volume 1, pp. 155–164. [\[CrossRef\]](#)
10. Poulain, T.; Mendez, J.; Henaff, G.; De Baglion, L. Influence of surface finish in fatigue design of nuclear power plant components. *Procedia Eng.* **2013**, *66*, 233–239. [\[CrossRef\]](#)
11. Le Duff, J.; Lefrançois, A.; Vernot, J. Effects of Surface Finish and Loading Conditions on the Low Cycle Fatigue Behavior of Austenitic Stainless Steel in PWR Environment Comparison of LCF Test Results with NUREG/CR-6909 Life Estimations. In Proceedings of the ASME 2008 Pressure Vessels and Piping Conference, Chicago, IL, USA, 27–31 July 2008; Volume 3, pp. 451–460. [\[CrossRef\]](#)
12. Du, D.; Wang, J.; Chen, K.; Zhang, L.; Andresen, P. Environmentally assisted cracking of forged 316LN stainless steel and its weld in high temperature water. *Corros. Sci.* **2019**, *147*, 69–80. [\[CrossRef\]](#)
13. Ertugrul Karabaki, H.; Solin, J.; Twite, M.; Herbst, M.; Mann, J.; Burke, G. Fatigue with hold times simulating NPP normal operation results for stainless steel grades 304L and 347. In Proceedings of the ASME 2017 Pressure Vessels & Piping Conference, Waikoloa, HI, USA, 16–20 July 2017 [\[CrossRef\]](#)
14. Coult, B.; Griffiths, A.; Beswick, J.; Gill, P.; Platts, N.; Smith, J.; Stevens, G. Results from environmentally-assisted short crack fatigue testing on austenitic stainless steels. In Proceedings of the ASME 2020 Pressure Vessels & Piping Conference, Online, 3 August 2020; PVP2020-21406. [\[CrossRef\]](#)
15. Métais, T.; Karabaki, E.; De Baglion, L.; Solin, J.; Le Roux, J.C.; Reese, S.; Courtin, S. European contributions to environmental fatigue issues experimental research in France, Germany & Finland. In Proceedings of the ASME Pressure Vessels and Piping Conference, Anaheim, CA, USA, 20–24 July 2014; Volume 1. [\[CrossRef\]](#)
16. Le Duff, J.; Lefrançois, A.; Vernot, J. Effects of surface finish and loading conditions on the low cycle fatigue behavior of austenitic stainless steel in PWR environment for various strain amplitude levels. In Proceedings of the ASME Pressure Vessels and Piping Conference, Prague, Czech, 26–30 July 2009; PVP2009-78129; Volume 3, pp. 603–610.
17. Mottershead, K.; Bruchhausen, M.; Cicero, S.; Cuvilliez, S. INCEFA-PLUS (Increasing Safety in NPPs by covering gaps in environmental fatigue assessment). In Proceedings of the ASME 2020 Pressure Vessels & Piping Conference, Online, 3 August 2020; PVP2020-21220. [\[CrossRef\]](#)
18. Cuvilliez, S.; McLennan, A.; Mottershead, K.; Mann, J.; Bruchhausen, M. Incefa-Plus Project: Lessons Learned From the Project Data and Impact On Existing Fatigue Assessment Procedures. *J. Press. Vessel. Technol.* **2020**, *2020*, 061507. [\[CrossRef\]](#)
19. Mottershead, K.; Bruchhausen, M.; Cuvilliez, S.; Cicero, S. Incefa-plus (increasing safety in NPPs by covering gaps in environmental fatigue assessment). In Proceedings of the ASME Pressure Vessels and Piping Conference, Prague, Czech, 15–20 July 2018; PVP2018-84034; Volume 1A. [\[CrossRef\]](#)
20. Spätig, P.; le Roux, J.C.; Bruchhausen, M.; Mottershead, K. Mean stress effect on fatigue life of 304L austenitic steel in air and PWR environments determined with strain and load controlled experiments. *Metals* **2021**, *11*, 221. [\[CrossRef\]](#)
21. ISO. ISO 12106:2017. *Metallic Materials — Fatigue Testing — Axial-Strain-Controlled Method*; ISO: Geneva, Switzerland, 2017.
22. ASTM. ASTM International E606 / E606M-19e1. *Standard Test Methods for Strain-Controlled Fatigue Testing*; ASTM: West Conshohocken, PA, USA, 2019.
23. ISO. ISO 11782-1:1998. *Corrosion of metals and alloys—Corrosion fatigue testing—Part 1: Cycles to failure testing*; ISO: Geneva, Switzerland, 1998; confirmed in 2019.
24. British Standards Institute (BSI). *BS 7270:2006 Metallic Materials. Constant Amplitude Strain Controlled Axial Fatigue*; Method of Test: 2006; British Standards Institute (BSI): London, UK 2015.
25. ISO. AFNOR A03-403. *Produits Métalliques—Pratique des Essais de Fatigue Oligocyclique*; ISO: Geneva, Switzerland, 2019; superseded by ISO in 2016.
26. Vankeerberghen, M.; Bruchhausen, M.; Cicero, R.; Doremus, L.; Roux, J.C.L.; Platts, N.; Spätig, P.; Twite, M.; Mottershead, K. Ensuring data quality for environmental fatigue—INCEFA-PLUS testing procedure and data evaluation. In Proceedings of the ASME Pressure Vessels and Piping Conference, Prague, Czech, 15–20 July 2018; PVP2018-84081; Volume 1A. [\[CrossRef\]](#)
27. Huotilainen, C.; Lydman, J. *D2.22 Microstructural Analysis of the Tested Outlier Specimens*; INCEFA-PLUS Project Deliverable; VVT: Espoo, Finland, 2020.
28. Gourdin, C.; Perez, G.; Dhahri, H.; Baglion, L.D.; le Roux, J.C. Environmental Effect On Fatigue Crack Initiation Under Equi-biaxial Loading of an Austenitic Stainless Steel. *Metals* **2021**, *11*, 203. [\[CrossRef\]](#)
29. Bruchhausen, M.; Mottershead, K.; Hurley, C.; Métais, T.; Cicero, R.; Vankeerberghen, M.; Le Roux, J.C. *Establishing a Multi-Laboratory Test Plan for Environmentally Assisted Fatigue*; ASTM Special Technical Publication; ASTM: West Conshohocken, PA, USA, 2017; Volume STP 1598, pp. 1–18. [\[CrossRef\]](#)
30. ISO. ISO 4287:1997. *Geometrical Product Specifications (GPS) — Surface Texture: Profile Method—Terms, Definitions and Surface Texture Parameters*; ISO: Geneva, Switzerland, 1997; under review.

31. ISO. *ISO 4288:1997. Geometrical Product Specifications (GPS)—Surface Texture: Profile Method—Rules and Procedures for the Assessment of Surface Texture*; ISO: Geneva, Switzerland, 1997.
32. Bruchhausen, M. *Fatigue Data from the INCEFA+ Main Programme, Version 1.0*; European Commission JRC: Brussels, Belgium, 2020. [[CrossRef](#)]
33. Twite, M.; Platts, N.; McLennan, A.; Meldrum, J.; McMinn, A. Variations in Measured Fatigue Life in LWR Coolant Environments due to Different Small Specimen Geometries. In Proceedings of the ASME Pressure Vessels & Piping Conference, Vancouver, BC, Canada, 17–21 July 2016; Volume 1A.
34. Asada, S.; Tsutsumi, K.; Fukuta, Y.; Kanasaki, H. Applicability of hollow cylindrical specimens to environmental assisted fatigue tests. In Proceedings of the ASME Pressure Vessels and Piping Conference, Waikoloa, HI, USA, 16–20 July 2017; PVP2017-65514; Volume 1A-2017.
35. Gill, P.; James, P.; Currie, C.; Madew, C.; Morley, A. An investigation into the lifetimes of solid and hollow fatigue endurance specimens using cyclic hardening material models in finite element analysis. In Proceedings of the ASME Pressure Vessels and Piping Conference, Waikoloa, HI, USA, 16–20 July 2017; Volume 1A-2017, PVP2017.
36. McLennan, A.; Spätig, P.; Roux, J.C.L.; Waters, J.; P. Gill, J.B.; Platts, N. INCEFA-PLUS project: The impact of using fatigue data generated from multiple specimen geometries on the outcome of a regression analysis. In Proceedings of the ASME 2020 Pressure Vessels & Piping Conference, Online, 3 August 2020; PVP2020-21422. [[CrossRef](#)]
37. ISO. *ISO 12107:2012(E). Metallic Materials—Fatigue Testing—Statistical Planning and Analysis of Data*; ISO: Geneva, Switzerland, 2012.
38. JMP15 Help. Available online: <https://www.jmp.com/support/help/en/15.2/#page/jmp/estimation-method-options.shtml#ww3555631> (accessed on 5 November 2020).
39. JMP15 Help. Available online: <https://www.jmp.com/support/help/en/15.2/#page/jmp/solution-path.shtml#ww488356> (accessed on 29 October 2020).
40. Bruchhausen, M.; McLennan, A.; Cicero, R.; Huotilainen, C.; Mottershead, K.; Le Roux, J.C.; Vankeerberghen, M. Environmentally Assisted Fatigue Data from the INCEFA-PLUS Project. In Proceedings of the ASME Pressure Vessels & Piping Conference, San Antonio, TX, USA, 14–19 July 2019; PVP2019-93085.
41. Bruchhausen, M. *Fatigue Data from the INCEFA+ Low Fen Programme, Version 1.0*; European Commission JRC: Brussels, Belgium, 2020. [[CrossRef](#)]
42. Dundulis, G.; Grybenas, A.; Bruchhausen, M.; Cicero, R.; Mottershead, K.; Huotilainen, C.; Le-Roux, J.C.; Vankeerberghen, M. INCEFA-PLUS project: review of the test programme and main results. In Proceedings of the 29th International Conference on Metallurgy and Materials, Online, 3 August 2020; pp. 410–415.
43. Bruchhausen, M. *Fatigue Data from the INCEFA+ Programme on Hold-Time Effects, version 1.0*; European Commission JRC: Brussels, Belgium, 2020. [[CrossRef](#)]